

COLOR MULTISCALE TEXTURE CLASSIFICATION OF HYSTEROSCOPY IMAGES OF THE ENDOMETRIUM

M. S. Neofytou¹, *Student Member, IEEE*, V. Tanos², M. S. Pattichis³, *Sen. Member, IEEE*, E. C. Kyriacou⁴, *Member, IEEE*, C. S. Pattichis¹, *Sen. Member, IEEE*, C. N. Schizas¹, *Sen. Member, IEEE*

Abstract—The objective of this study was to investigate the diagnostic performance of a Computer Aided Diagnostic (CAD) system based on color multiscale texture analysis for the classification of hysteroscopy images of the endometrium, in support of the early detection of gynaecological cancer. A total of 416 Regions of Interest (ROIs) of the endometrium were extracted (208 normal and 208 abnormal) from 45 subjects. RGB images were gamma corrected and were converted to the YCrCb color system. The following texture features were extracted from the Y, Cr and Cb channels: (i) Statistical Features (SF), (ii) Spatial Gray Level Dependence Matrices (SGLDM), and (iii) Gray Level Difference Statistics (GLDS). The Probabilistic Neural Network (PNN), statistical learning and the Support Vector Machine (SVM) neural network classifiers were also applied for the investigation of classifying normal and abnormal ROIs in different scales.

Results showed that the highest percentage of correct classification (%CC) score was 79% and was achieved for the SVM models trained with the SF and GLDS features for the 1x1 scale. This %CC was higher by only 2% when compared with the CAD system developed, based on the SF and GLDS feature sets computed from the Y channel only. Further increase in scale from 2x2 to 9x9, dropped the %CC in the region of 60% for the SF, SGLDM, and GLDS, feature sets, and their combinations. Concluding, a CAD system based on texture analysis and SVM models can be used to classify normal and abnormal endometrium tissue in difficult cases of gynaecological cancer. The proposed system has to be investigated with more cases before it is applied in clinical practise.

Keywords—Hysteroscopy imaging, gynaecological cancer, texture analysis, color multiscale analysis, endometrium.

I. INTRODUCTION

Hysteroscopy is considered to be the gold-standard technique for the diagnosis of intrauterine pathology [1]. The physician guides the telescope connected to a camera inside the endometrium in order to investigate suspicious lesions of cancer [2]. A standardized protocol based on color imaging correction and texture feature extraction enabling the quantitative analysis for the assessment of gynaecological tissue in hysteroscopy imaging was published by our group [3]. Using this protocol, a Computer

Aided Diagnostic (CAD) system was developed also by our group for the classification of normal and abnormal ROIs of the endometrium from hysteroscopy images [4].

This system was based on the SF and GLDS texture analysis feature sets computed for the Y channel only where the highest percentage of correct classifications (%CC) score was 77%. The same system was also investigated but for the YCrCb space, for the SF and SGLDS feature sets where the highest %CC was 79% [5]. The objective of this new study is to investigate the diagnostic performance of a CAD system based on color multiscale texture analysis (for scales 1x1 to 9x9) for the classification of hysteroscopy images of normal and abnormal endometrium, in support of the early detection of gynaecological cancer.

To the best of our knowledge, no similar study was carried out for hysteroscopic imaging of the endometrium. Gray-level texture analysis is widely used in numerous image processing and analysis tasks [5]. New studies, exploiting the usefulness of color texture have been presented by several researchers [6], [7]. In laryngoscopic imaging [8], suspect lesions were analyzed automatically using co-occurrence matrices with color differences between neighbouring pixels. A novel methodology for the extraction of color image features in colonoscopic video processing for the detection of colorectal polyps was developed in [9]. They utilized the covariances of the second-order statistical measures calculated over the wavelet transformation of different color bands. The rest of the paper is organized into four sections. In sections II, III and IV we present the methodology, results and concluding remarks respectively.

II. METHODOLOGY

A. Video Recording

The CIRCON IP4.1 [10] medical camera was used. The analog output signal of the camera (PAL 475 horizontal lines) was digitized at 720x576 pixels using 24 bits color at 25 frames per second, and was then saved in the AVI format. The Digital Video Creator 120 frame grabber was used [11].

B. Material

A total of 416 RGB hysteroscopy images from the endometrium were recorded from 45 subjects. ROIs of 64x64 pixels were manually cropped and classified into two categories: (i) normal ROIs (N=208) and (ii) abnormal ROIs (N=208) based on the physician's subjective criteria and the histopathological examination (see Fig. 1).

Manuscript received April 7, 2008.

¹Dep. of Computer Science, University of Cyprus, Nicosia, Cyprus, {mneoph, schizas, pattichis}@ucy.ac.cy

²Aretaeon Hospital, Nicosia, Cyprus, v.tanos@aretaeo.com

³Dep. of Electrical and Computer Engineering, University of New Mexico, NM, USA, pattichis@ecece.unm.edu

⁴Dep. of Computer Science and Engineering, Frederick University, Nicosia, Cyprus, ekyriac@ucy.ac.cy

C. Transformation of RGB to YCrCb

All RGB images were transformed to the YCrCb color system. This transformation was implemented using [12]:

$$\begin{bmatrix} Y \\ Cr \\ Cb \end{bmatrix} = \begin{bmatrix} 0.299 & 0.587 & 0.114 \\ 0.596 & -0.275 & -0.321 \\ 0.212 & -0.523 & 0.311 \end{bmatrix} \begin{bmatrix} R \\ G \\ B \end{bmatrix} \quad (1)$$

In Fig. 1, we present in up-left the original RGB image of the endometrium and in up-right, down-left, down-right the transformed Y, Cr, and Cb images based on eq. (1).

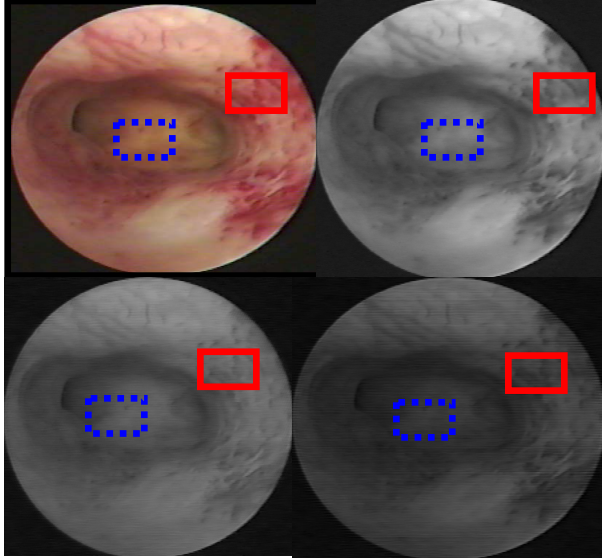


Fig. 1. Endometrium images in (left to right) RGB, Y, Cr, and Cb space. Dotted blue and solid red boxes represent normal and abnormal ROIs respectively.

D. Multiscale analysis

The goal of multiscale image analysis is to reveal image characteristics at different image resolutions. For example, small objects affect texture features at low resolution levels (with little or no downsampling involved because the information is centralized in all image), while larger objects affect texture features at higher resolution levels. Thus, if there is a particular range of scales, where we have objects

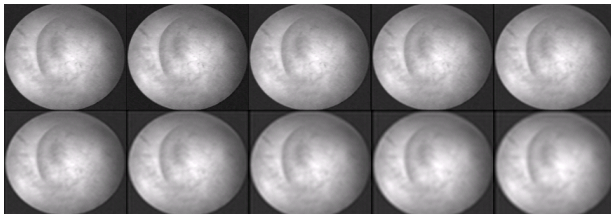


Fig. 2. Multiscale analysis of an endometrium gray scale image. Upper row: original image and images with downsampling rates 2x2 up to 5x5. Lower row: images with downsampling rates 6x6 up to 10x10.

of diagnostic interest, it is preferable to use this range for feature extraction in CAD systems. Within a single image scale, there is a number of different frequency bands that can be used for texture feature analysis.

In this study, we only used the lowest frequency band. This was implemented by first applying a low-pass filter, followed by downsampling by a factor of 2 to 10 in each direction as illustrated in Fig. 2. Thus, our approach is closely related to generate a scale space, where the input image is convolved with Gaussians of different spreads.

We note that significant differences exist between the downsampled images of Fig. 2. Yet, it is not easy to observe these differences without a very careful examination. In this study, texture features were computed for each the YCrCb channels for the scales 1x1, 2x2, 4x4, and 9x9.

E. Feature Extraction

The following texture features were extracted for the Y, Cr, and Cb channels.

Statistical Features (SF): SF features describe the gray level histogram distribution without considering spatial independence. The following texture features were computed: 1) Mean, 2) Variance, 3) Median, 4) Mode, 5) Skewness, 6) Kurtosis, 7) Energy and 8) Entropy.

Spatial Gray Level Dependence Matrices (SGLDM): The spatial gray level dependence matrices as proposed by Haralick et al. [13] are based on the estimation of the second-order joint conditional probability density functions that two pixels (k, l) and (m, n) with distance d in direction specified by the angle θ , have intensities of gray level i and gray level j . Based on the estimated probability density functions, the following 13 texture measures proposed by Haralick et al. were computed: 1) ASM, 2) Contrast, 3) Correlation, 4) Variance, 5) Homogeneity, 6) Sum Average, 7) Sun Variance, 8) Entropy, 9) Sum Entropy, 10) Dif. Variance, 11) Dif. Entropy, 12) Inf. Correlation1, and 13) Inf. Correlation2.

Gray level difference statistics (GLDS): The GLDS algorithm [14], [15] is based on the assumption that useful texture information can be extracted using first order statistics of an image. The algorithm is based on the estimation of the probability density p_δ of image pixel pairs at a given distance $\delta=(\Delta_x, \Delta_y)$, having a certain absolute gray level difference value. Coarse texture images, result in low gray level difference values, whereas, fine texture images result interpixel gray level differences with great variances. The following features were computed: 1) Homogeneity, 2) Contrast, 2) Energy, 4) Entropy and 5) Mean.

F. Image Classification

The diagnostic performance of the texture features was evaluated with two different classifiers: the Probabilistic Neural Network (PNN), and the Support Vector Machine (SVM). These classifiers were trained to classify the texture features into two classes: i) normal ROIs or ii) abnormal ROIs. The PNN [16] classifier is basically a kind of Radial Basis Function (RBF) network. This classifier was investigated for several spread radii in order to identify the best for the current problem. The SVM network was investigated using the Gaussian Radial Basis Function

(RBF) kernels; this was decided as the rest of the kernel functions could not achieve so good results. The SVM with RBF kernel was investigated using 10-fold cross validation in order to identify the best parameters such as spread of the RBF kernels. The leave-one-out method was used for validating all the classification models. A total of 3X416 runs were carried out for training the classifiers, and the performance of the classifiers was evaluated on the remaining one subset. The runs were done in each of the three color systems. The performance of the classifier systems were measured using the parameters of the receiver operating characteristic (ROC) curves. We also computed the percentage of correct classifications ratio (%CC) based on the correctly and incorrectly classified cases.

III. RESULTS

Table I presents the Median and Semi Inter Quartile Range (SIQR) from selected texture features and statistical analysis for the Y, Cr and Cb channels. It is clearly shown that there was a significant difference for all texture features tabulated for normal vs abnormal ROIs of the endometrium for the Y channel but not for the Cr and Cb channels.

As shown in Table I for the Y channel, abnormal ROIs had higher variance, but with smaller differences for the Cr and Cb channels. Also abnormal ROIs had lower median and contrast values when compared to the normal ROIs in the Y channel. There was no significant difference for the median and contrast features for the Cr and Cb channels.

Table II presents the performance of the SVM and PNN CAD system investigated for classifying normal vs. abnormal endometrium tissue for the following scales: 1x1, 2x2, 4x4 and 9x9 without using PCA. We also classify using the SF, SGLDM and GLDS features sets for the YCrCb color system.

It is clearly shown in Table II that the SVM classifier performed better than the PNN classifier. For the SVM classifier, the best performance was achieved for the models of scale 1x1 for the SF+GLDS feature sets in the YCrCb system with %CC=79, followed by the SF+SGLDM+GLDS feature sets in the same system with %CC=77. The combination of the different texture features for the YCrCb system slightly improved the %CC. Similar performance was obtained when using only the Y channel features (%CC=77, see [5]). Further increase in scale from 2x2 to 9x9, dropped significantly the %CC in the region of 60% for the SF SGLDM, GLDS, feature sets, and their combinations.

IV. CONCLUDING REMARKS

In this study, a CAD system based on color multiscale texture analysis for the classification of hysteroscopy images of the endometrium, in support of the early detection of gynaecological cancer was investigated. There was a significant difference for most of the SF, SGLDM, and GLDS texture features investigated between the normal and abnormal ROIs for all scales for the Y channel.

The highest percentage of correct classifications score was %CC=79 and was achieved for the SVM classifier for the SF+GLDS feature sets in the YCrCb system in the 1x1 scale. This %CC was higher by only 2% when compared with the CAD system developed based on the SF+GLDS feature sets computed from the Y channel only. Further increase in scale from 2x2 to 9x9, dropped significantly the %CC in the region of 61% for the SF, SGLDM, and GLDS, feature sets, and their combinations because of the destroyed information of the image after the downsampling.

ACKNOWLEDGMENT

This study is funded through the Research Promotion Foundation, Cyprus, PENEK 2005, through the project entitled: "Intraoperative Computer Assisted Tissue Image Analysis" (CATIA), April 2006 – April 2008.

REFERENCES

- [1] Fayeze, M.F. Vogel, "Comparison of different treatment methods of endometriomas by laparoscopy," *Obstet. Gynecol.*, Vol. 78, pp. 660-665, 1991.
- [2] R. Wenzl, R. Lehner, U. Vry, N. Pateisky, P. Sevelde, P. Husslein, "Three-dimensional video-hysteroscopy: clinical use in gynaecological laparoscopy," *Lancet*, Vol. 344, pp. 1621-1622, 1994.
- [3] M.S. Neofytou, C.S. Pattichis, M.S. Pattichis, V. Tanos, E.C. Kyriacou, D. Koutsouris, "A Standardised Protocol for Texture Feature Analysis of Endoscopic Images in Gynaecological Cancer," *BioMedical Engineering OnLine*, <http://www.biomedical-engineering-online.com/content/6/1/44>, *BioMedical Engineering OnLine* 2007, 6:44.
- [4] M.S. Neofytou, C.S. Pattichis, M.S. Pattichis, V. Tanos, E.C. Kyriacou, D. Koutsouris, "Texture-Based Classification of Hysteroscopy Images of the Endometrium," 28th Annual International conference of the IEEE engineering in Medicine and Biology Society, 30-3 August, September, New York, USA, pp.3005-3008, 2006.
- [5] M.S. Neofytou, C.S. Pattichis, M.S. Pattichis, V. Tanos, E.C. Kyriacou, S. Pavlopoulos, "Color-Texture Classification of Hysteroscopy Images of the Endometrium," 29th Annual International conference of the IEEE engineering in Medicine and Biology Society, 23-26 August, Lyon, France, pp. 864-867, 2007.
- [6] R.M. Haralick, "Statistical and structural approaches to texture," *Proc. IEEE*, vol. 67, pp. 786-804, 1979.
- [7] *The Handbook of Pattern Recognition and Computer Vision*, 2nd ed., C.H. Chen, L.F. Pau, and P.S. P.Wang, Eds., World Scientific, Singapore, 1998, pp. 207-248.
- [8] F. R. J. Ilgner, P. Christoph, G. S. Andreas, S. Klaus, M. Westhofen T. M. Lehmann, "Colour Texture Analysis for Quantitative Laryngoscopy," *Acta Otolaryngol*, vol. 123, pp. 730-734, 2003.
- [9] S. A. Karkanis, D. K. Iakovidis, D. E. Maroulis, D. A. Karras, M. Tzivras, "Computer-Aided Tumor Detection in Endoscopic Video Using Color Wavelet Features," *IEEE Trans. on Info. Tech. in Biom.*, Vol. 7, no. 3, Sempptember 2003.
- [10] Web link: <http://www.acmicorp.com>
- [11] Web link: <http://www.pinnaclesys.com>
- [12] Web link: <http://www.mathworks.com>
- [13] R.M. Haralick, K. Shanmugam, I. Dinstein, "Texture Features for Image Classification," *IEEE Trans. on Systems, Man., and Cybernetics*, Vol. SMC-3, pp. 610-621, Nov. 1973.
- [14] C.M. Wu, Y.C. Chen, and K.S. Hsieh, "Texture features for classification of ultrasonic liver images," *IEEE Trans. Med. Imaging*, vol. 11, pp. 141-152, 1992.
- [15] J.S. Wenska, C.R. Dryer, and A. Rosenfeld, "A comparative study of texture measures for terrain classification," *IEEE Trans. Syst., Man, Cyber.*, vol. SMC-6, pp. 269-285, 1976.
- [16] D.F. Specht, Probabilistic Neural Networks, *INNS Neural Networks* 3(1), 109-118, 1990.

TABLE I: SELECTED TEXTURE FEATURES FOR THE SF, SGLDM AND GLDS FEATURE SETS FOR THE Y, Cr AND Cb CHANNELS FOR SCALE 2X2 (MEDIAN AND THE SEMI INTER QUARTILE RANGE (SIQR)). H=WILCOXON RANK SUM TEST, *1=SIG. DIFF., *0=NO SIG. DIFF., a=0.05.

	Y Channel			Cr Channel			Cb Channel		
	Normal	Abnormal	H	Normal	Abnormal	H	Normal	Abnormal	H
	Median	SIQR		Median	SIQR		Median	SIQR	
SF									
Mean	167	156	13	184	85	183	0,25	0	180
Variance	984	1116	223	880	328	895	7	1	926
Median	171	160	15	188	87	188	0,06	0	184
SGLDM									
Contrast	1000	922	156	1156	500	1142	7	1	1247
Variance	753	999	249	608	179	624	8	1	666
Entropy	6,93	7,15	0,11	6,56	3,22	6,7	0,07	1	4,27
GLDS									
Homogeneity	0,16	0,13	0,02	0,16	0,07	0,15	0,002	1	0,1
Contrast	995	917	155	1150	497	1136	7	1	1240

TABLE II: CLASSIFICATION PERFORMANCE OF THE SVM (PNN) MODELS FOR THE CLASSIFICATION OF THE ENDOMETRIUM BASED ON TEXTURE FEATURES FOR THE YCrCb SYSTEMS FOR SCALES: 1X1, 2X2, 4X4 AND 9X9.

SVM (PNN) classifier, YCrCb, Scale 1x1	%CC	%FP	%FN	%SE	%SP	%PR
SF	73 (68)	21 (11)	31 (51)	68 (48)	78 (88)	76 (81)
SGLDM	74 (69)	28 (14)	23 (47)	76 (52)	71 (85)	72 (78)
GLDS	75 (68)	24 (13)	25 (50)	75 (49)	75 (86)	75 (78)
SF+SGLDM	76 (70)	25 (13)	22 (46)	77 (53)	75 (86)	75 (79)
SF+GLDS	79 (69)	25 (12)	16 (48)	83 (51)	74 (87)	76 (81)
SGLDM+GLDS	76 (69)	25 (15)	23 (46)	76 (53)	75 (84)	75 (77)
SF+SGLDM+GLDS	77 (70)	25 (15)	20 (44)	79 (55)	74 (84)	75 (78)
SVM (PNN) classifier, YCrCb, Scale 2x2						
SF	58 (56)	32 (14)	52 (73)	48 (27)	68 (86)	60 (65)
SGLDM	60 (58)	34 (16)	46 (67)	54 (33)	66 (84)	61 (67)
GLDS	61 (54)	31 (34)	48 (57)	52 (43)	69 (66)	63 (56)
SF+SGLDM	60 (58)	29 (17)	52 (68)	48 (32)	71 (83)	63 (66)
SF+GLDS	61 (57)	29 (15)	50 (70)	50 (30)	71 (85)	64 (67)
SGLDM+GLDS	60 (57)	29 (21)	50 (64)	50 (36)	71 (79)	63 (63)
SF+SGLDM+GLDS	61 (58)	31 (18)	47 (66)	53 (34)	69 (82)	63 (65)
SVM (PNN) classifier, YCrCb, Scale 4x4						
SF	60 (55)	29 (8)	51 (82)	49 (18)	71 (92)	62 (69)
SGLDM	60 (57)	26 (12)	55 (74)	45 (26)	74 (88)	64 (69)
GLDS	59 (54)	21 (6)	63 (86)	38 (14)	79 (94)	64 (71)
SF+SGLDM	59 (57)	23 (11)	58 (75)	42 (25)	77 (89)	65 (70)
SF+GLDS	59 (56)	26 (6)	57 (82)	43 (18)	74 (94)	63 (74)
SGLDM+GLDS	60 (58)	27 (10)	52 (75)	48 (25)	73 (90)	64 (72)
SF+SGLDM+GLDS	60 (57)	27 (10)	52 (76)	48 (24)	73 (90)	64 (70)
SVM (PNN) classifier, YCrCb, Scale 9x9						
SF	57 (54)	25 (12)	61 (80)	39 (20)	75 (88)	61 (63)
SGLDM	61 (54)	24 (29)	54 (62)	46 (38)	76 (71)	65 (57)
GLDS	61 (54)	30 (42)	48 (50)	52 (50)	70 (58)	64 (54)
SF+SGLDM	60 (55)	29 (24)	52 (67)	48 (33)	71 (76)	63 (58)
SF+GLDS	61 (55)	32 (20)	47 (71)	53 (29)	68 (80)	63 (60)
SGLDM+GLDS	61 (55)	29 (35)	50 (56)	50 (44)	71 (65)	63 (56)
SF+SGLDM+GLDS	59 (54)	37 (29)	46 (62)	54 (38)	63 (71)	60 (57)